

## PHYSICAL PROCESSES IN PHOTON-STARVED NONTHERMAL PAIR PLASMAS

ANDRZEJ A. ZDZIARSKI

Space Telescope Science Institute; and California Institute of Technology

PAOLO S. COPPI

California Institute of Technology; and Space Telescope Science Institute

AND

DON Q. LAMB

Department of Astronomy and Astrophysics and Enrico Fermi Institute, University of Chicago

Received 1986 September 24; accepted 1989 December 28

### ABSTRACT

We study Compton spectra produced by relativistic unmagnetized nonthermal electron-positron pairs injected into “photon-starved” plasmas, i.e., plasmas where the luminosity in soft photons is much less than the power in the nonthermal pair injection. The main physical processes in photon-starved plasmas are: the repeated Compton scattering of individual photons before they escape the source, production of electron-positron pairs in photon-photon collisions, the cooling of pairs to an equilibrium temperature and the formation of the thermal plasma component, and the transfer of energy from the nonthermal pairs to thermal ones via Coulomb collisions. We find the equilibrium temperature is often relativistic and increases with the decreasing compactness parameter  $L_e/R$ , where  $L_e$  and  $R$  are the luminosity in injected electron pairs and radius, respectively. Coulomb interactions are important in such plasmas and may transfer a large fraction of the injected nonthermal power directly to the thermal component, which keeps the Thomson optical depth of the nonthermal component small. For small enough soft photon luminosities, bremsstrahlung emission by the thermal and nonthermal electrons becomes important.

When the compactness in pairs is low, the X-ray photon spectrum is due mostly to moderately Comptonized thermal bremsstrahlung from the semirelativistic plasma; when the compactness is high, it is due to repeated Compton upscattering of soft photons on a cool, optically thick thermal plasma. The overall spectra are very hard in the X-ray range, peak near 0.1–1 MeV, and are cut off at higher energies with power-law tails following the cutoffs. Such spectra are relevant to theoretical models of gamma-ray bursts, active galactic nuclei, and the cosmic X-ray and gamma-ray backgrounds.

*Subject headings:* gamma rays: bursts — radiation mechanisms

### I. INTRODUCTION

We study here nonthermal unmagnetized relativistic plasmas in pair equilibrium. The assumptions adopted in this work are similar to those of Zdziarski and Lightman (1985), Zdziarski and Lamb (1986, hereafter ZL86), Fabian *et al.* (1986), Svensson (1987), Lightman and Zdziarski (1987, hereafter LZ87), and Done and Fabian (1989). The basic assumption of those papers as well as of the present work is that a fraction of the available energy is supplied to the isotropic and homogeneous plasma in the form of a flux of relativistic electrons or pairs (nonthermal injection). These injected relativistic pairs lose their energy mostly via Compton scattering of soft photons. The resulting radiation spectrum extends above the threshold for production of  $e^+e^-$  pairs, 511 keV. The produced pairs can Compton scatter as well, giving rise to an  $e^+e^-$  pair cascade. In steady state, the pair production rate equals the sum of the pair annihilation and pair escape rates (pair equilibrium). For reviews of such pair plasmas and a comparison of their emitted photon spectra to those of cosmic compact objects, see Svensson (1986), Zdziarski and Lightman (1987), and Svensson and Zdziarski (1989).

The work presented here concentrates on the case of the photon-starved or photon-deficient plasmas. We will define such plasmas as those where the luminosity in any sources of soft ( $h\nu \lesssim m_e c^2$ ) photons,  $L_s$ , is much less than the power injected in the primary relativistic electrons,  $L_e$ —so much that

the power radiated away by the photons after a single scattering off the cooled nonthermal electron distribution is also much less than the injected power in primary electrons. Since the escaping photon luminosity must balance the total injected luminosity in a steady state, it follows that repeated scatterings of photons by either thermal or nonthermal electrons have to be important in such cases. Moreover, the spectra of photon-starved plasmas will be hard (i.e., most photons emerge with significantly higher energies than they were injected with), since the luminosity injected in pairs must make its way to the photon distribution (via repeated Compton upscattering). Because of this deficit of soft photons, the Compton cooling times for injected pairs are not necessarily much shorter than other time scales relevant to the problem. Slower processes such as Coulomb cooling and electron-electron bremsstrahlung can then have a significant impact on the equilibrium particle distributions.

There are several effects specific to photon-starved plasmas. First, higher order Compton scattering are important by the definition above. A typical primary photon will get upscattered several times before leaving the source.

Second, the relativistic electrons cool on the upscattered spectrum rather than on the (deficient) primary soft photons. Typically, the upscattered spectrum extends to high energies. Many Compton scatterings are in the Klein-Nishina regime ( $\epsilon\gamma > 1$ , where  $\gamma$  is the electron Lorentz factor and  $\epsilon$  is the

photon energy in units of the electron rest mass,  $\epsilon \equiv hv/m_e c^2$ , and Klein-Nishina corrections can no longer be ignored. In particular, the use of a Klein-Nishina cutoff for the scattering rate (e.g., as in LZ87) becomes inappropriate (see Coppi and Blandford 1990, hereafter CB90). Also, the evolution of the pair distribution will no longer be well described by the continuous cooling approximation,  $dN(\gamma)/dt = -(d/d\gamma)[\dot{\gamma}N(\gamma)]$ . Here  $\dot{\gamma}$  is the cooling rate, and  $N$  is the nonthermal pair distribution function. In the Klein-Nishina regime, pairs lose energy in large, discrete steps (Blumenthal and Gould 1970; Zdziarski 1988).

Third, the equilibrium temperature,  $\Theta$ , to which the relativistic electrons cool, will be high ( $\Theta \lesssim 1$ ), and the associated Compton parameter  $\gamma$  will be large ( $> 1$ ). Here  $\Theta \equiv kT/m_e c^2$  is the dimensionless electron temperature. The Compton parameter, determining the efficiency of Comptonization by thermal electrons, is given by equation (16) below.

We study here plasmas with negligible magnetic fields. The injected particles are taken to be  $e^+e^-$  pairs. We consider only steady (stationary) plasmas where the sum of the injection rate and the rate of pair production by photons equals the sum of the rate of  $e^+e^-$  pair annihilation and the rate of escape of pairs from the plasma. For the process of Compton scattering, we assume that some contribution to the cooling rate is from Compton scattering in the classical Thomson regime. (See studies of pair cascades in the regime where the injection occurs in the extreme Klein-Nishina regime, e.g., Zdziarski 1988).

Photon-deficient plasmas without magnetic fields were studied before by ZL86, LZ87, and Done and Fabian (1989). In contrast to those papers, we include the process of Coulomb energy loss of the relativistic electrons to the background thermal plasmas. We find the process to be important in a wide range of plasma parameters (see also de Kool and Begelman 1989; Dermes and Liang 1989). Its importance increases with decreasing compactness in the electron injection,  $l_e$ , and decreasing  $l_\gamma/l_e$ , the ratio of the soft photon and electron injection compactnesses. Here  $l$  is the compactness parameter,  $l \equiv L\sigma_T/Rm_e c^3$ , determining the importance of  $e^+e^-$  pair production and Compton losses in a source. The subscript  $e$  corresponds to the primary electron (or pair) injection, while  $s$  corresponds to the primary soft photons.

Our results differ somewhat from ZL86 as far as the  $\gamma$ -ray spectra from photon-deficient sources are concerned. ZL86 found that a typical spectrum was a broken power law with a low-energy spectral index  $\alpha_x < 1$  at  $\epsilon \lesssim 1$  and a high-energy spectral index  $\alpha_y > \alpha_x$  at  $\epsilon \gtrsim 1$ . Here the energy spectral index is defined as  $F_\nu \propto \nu^{-\alpha}$ . We find that Coulomb losses at low compactnesses and Compton losses at large compactnesses cause the optical depth of the nonthermal part of the electron distribution to be always  $\ll 1$ . This results in a diminished role of scattering by the nonthermal electrons and a spectral turnover at  $\epsilon \gtrsim 1$ . Beyond the turnover, the amplitude of the high-energy,  $\gamma$ -ray part of the spectrum is reduced. Also, the effects of Compton up- and downscattering by the thermal plasma and pair annihilation at  $l \gg 1$  result in additional structure in the spectrum at  $\epsilon \lesssim 1$ . These effects were not discussed in ZL86.

In the classification scheme of Svensson (1987), nonthermal electron-positron cascades of the type considered by ZL86, LZ87, and the present work fall into his type III. Those cascades are fully nonlinear, by which it is meant that both  $e^+e^-$  cooling and pair production occur on photons previously upscattered by the injected relativistic electrons.

One example of a physical situation where the soft photon luminosity,  $L_s$ , may be much less than the luminosity injected in relativistic electrons,  $L_e$ , is acceleration of electrons in a region which lies several stellar radii above a (weakly magnetized) neutron star. Then only a small fraction of  $L_e$  intercepts the stellar surface and is reemitted as blackbody radiation  $L_s$ , providing a source of soft photons in a self-consistent way (see ZL86). Another example is a source (in the vicinity of either a neutron star or a black hole) in which soft photons are produced by synchrotron emission in a magnetic field that is below the equipartition strength, or a source in which bremsstrahlung is the only source of photons.

We compare our theoretical spectra to the spectra of  $\gamma$ -ray bursts and active galactic nuclei (AGNs) (see § V). Some of the theoretical spectra resemble the spectra of some "classical"  $\gamma$ -ray bursts, and some resemble those of "soft  $\gamma$ -ray repeaters." They may also be relevant to the X-ray and  $\gamma$ -ray spectra of active galactic nuclei. In particular, photon-starved sources may be responsible for the  $\sim 1$  MeV peak observed in several AGNs and the cosmic  $\gamma$ -ray background (e.g., Bassani *et al.*, 1985). Photon-starved plasmas may also explain the spectral indices less than 0.5 observed in certain AGNs (e.g., Mushotzky 1984) and in the cosmic X-ray background (e.g., Marshall *et al.*, 1980).

## II. THE MODEL OF PHYSICAL PROCESSES

The treatment of the physical processes we use here is for the most part described in CB90. The method of solving nonlinear pair cascades is analogous to that of Coppi (1990, hereafter C90). For the present work, the main advantages of the method of CB90 and C90 compared to that of LZ87 are: (i) the exact Klein-Nishina Compton scattering rates are used, (ii) the electron kinetic equations are solved directly without relying on the continuity equation (see LZ87), and (iii) the method for treating thermal Comptonization works at relativistic temperatures. The processes we study here are Compton scattering, thermal and nonthermal pair annihilation, two-photon pair production, thermal and nonthermal bremsstrahlung, and Coulomb scattering. LZ87 did not include the effects of Coulomb collisions, bremsstrahlung, and nonthermal pair annihilation.

We assume that  $e^+e^-$  pairs are continuously injected at a rate  $Q(\gamma)$  particles per unit time per unit volume per unit energy, with  $\gamma_{\min} \leq \gamma \leq \gamma_{\max}$ . (This contrasts with ZL86 and LZ87, who took the injected particles to be electrons.) We assume that the injection occurs uniformly throughout a spherical volume of radius  $R$ . The total power  $L_e$  put into the primary pairs is measured by the dimensionless "pair compactness parameter,"

$$l_e \equiv \frac{L_e \sigma_T}{R m_e c^3} = \frac{4\pi \sigma_T R^2}{3c} \int_{\gamma_{\min}}^{\gamma_{\max}} \gamma Q(\gamma) d\gamma, \quad (1)$$

which is roughly proportional to the optical depth to  $e^+e^-$  pair production in photon-photon collisions. Here  $\sigma_T$  is the Thomson cross section, and  $m_e$  is the electron mass. The injected pairs eventually annihilate and contribute their rest-mass energy to the radiated photon spectrum. We therefore include their rest-mass energy in our definition of the power  $L_e$  (see eq. [2a] of LZ87). The form of the injection function  $Q(\gamma)$  is taken to be a power-law of index  $\Gamma$  extending from energies  $\gamma_{\min}$  to  $\gamma_{\max}$ .

One source of soft photons that is always present in a plasma is bremsstrahlung from both thermal and nonthermal

electrons. In addition, we assume for some models an injection of blackbody photons with dimensionless temperature  $\Theta_{bb}$  ( $\equiv kT_{bb}/m_e c^2$ ) at the rate  $\dot{n}_0$  photons per unit volume per unit energy  $\epsilon$ . We will take  $\Theta_{bb} = 10^{-4}$  to  $10^{-3}$  in our numerical models. We assume  $\Theta_{bb} \gamma_{\max} \leq 1$ , so that for any pair a nonzero part of the photon spectrum is in the Thomson limit. The “soft photon compactness” is

$$l_s \equiv \frac{L_s \sigma_T}{R m_e c^3} = \frac{4\pi \sigma_T R^2}{3c} \int_0^\infty \epsilon \dot{n}_0(\epsilon) d\epsilon. \quad (2)$$

The numerical value of the constant  $\sigma_T/m_e c^3$  in equations (1) and (2) is  $1/(3.7 \times 10^{28} \text{ ergs s}^{-1} \text{ cm}^{-2})$ . The photon injection is assumed uniform and isotropic throughout the source.

We divide the pair distribution into a thermal and a non-thermal population (some quantities related to those populations will have superscripts “th” and “nth,” respectively). Let  $n(\epsilon)$  and  $N(\gamma)$  be the number densities per unit energy of photons and nonthermal pairs, respectively, at a representative interior point of the emission region. The equation governing the nonthermal pair distribution,  $N$ , is then,

$$P(\gamma) + Q(\gamma) + \int_1^{\gamma_{\max}} N(\gamma') C(\gamma', \gamma) d\gamma' \\ = N(\gamma) \int_1^{\gamma_{\max}} C(\gamma, \gamma') d\gamma' + A^{\text{nth}}(\gamma) + \frac{\partial}{\partial \gamma} [(\dot{\gamma}_B + \dot{\gamma}_{\text{Coul}}) N(\gamma)]. \quad (3)$$

Here  $P(\gamma)$  is the rate of pair creation per unit volume per unit energy,  $Q(\gamma)$  is the rate of injection of primary pairs per unit volume per unit energy, and  $C(\gamma', \gamma)$  is the Compton transition rate for scattering from Lorentz factor  $\gamma'$  to  $\gamma$ , which depends on the photon spectrum,  $n$ . The  $A^{\text{nth}}$  is the rate of non-thermal annihilation (see CB90), which includes the contributions from both the thermal pairs and the other nonthermal pairs. The  $\dot{\gamma}_B$  and  $\dot{\gamma}_{\text{Coul}}$  are the cooling rates due to  $e^\pm e^\pm$  bremsstrahlung and Coulomb cooling, respectively. See CB90 for a more detailed discussion of these terms. Since their cooling time is less than  $R/c$  at  $l \gtrsim 1$ , pairs cannot leave the sources before cooling completely. Hence we do not include an escape term for the nonthermal pairs. Upon reaching the thermal range of energies, the nonthermal pairs are transferred to the thermal distribution (see discussion after eq. [16] below).

The thermal (Maxwell-Boltzmann) distribution has a dimensionless temperature  $\Theta$  and a Thomson optical depth  $\tau_T^{\text{th}} = (N_+ + N_-) \sigma_T R$ . Here  $N_+$ ,  $N_-$  are the densities of thermal positrons and electrons, respectively. We determine  $\Theta$  and  $\tau_T^{\text{th}}$  from energy balance and pair balance, respectively (see eqs. [15] and [13] below). We neglect here production of non-thermal electrons due to upscattering of thermal electrons by  $\gamma$ -rays. The energy transferred by the  $\gamma$ -rays in this process is added to the total energy of the thermal population (see eq. [15]).

The photon kinetic equation is

$$\dot{n}_0(\epsilon) + \dot{n}_A^{\text{nth}}(\epsilon) + \dot{n}_A^{\text{th}}(\epsilon) + \dot{n}_B^{\text{nth}}(\epsilon) + \dot{n}_C^{\text{nth}}(\epsilon) + \dot{n}_C^{\text{th}}(\epsilon) \\ = \frac{c}{R} n(\epsilon) [\tau_C^{\text{nth}}(\epsilon) + \tau_{\gamma\gamma}(\epsilon)] + \frac{c}{R} n(\epsilon) \left[ 1 + \frac{\tau_C^{\text{th}}(\epsilon)}{3} f(\epsilon) \right]^{-1}. \quad (4)$$

Here  $\dot{n}_0$ ,  $\dot{n}_A$ ,  $\dot{n}_B$ , and  $\dot{n}_C$  are the rates of production of photons at energy  $\epsilon$  by soft photon injection, pair annihilation, bremsstrahlung, Compton scattering off nonthermal electrons, and Compton scattering off thermal electrons, respectively. We treat pair annihilation, bremsstrahlung, and scattering by

thermal and nonthermal electrons separately (see CB90). Photons are removed from energy  $\epsilon$  by Compton scattering with nonthermal electrons, having Compton optical depth  $\tau_C^{\text{nth}}$  (calculated using the Klein-Nishina cross section and depending on the electron distribution  $N$ ), and by pair creation, having optical depth  $\tau_{\gamma\gamma}$ . The removal of photons due to Compton scattering with thermal electrons is included in  $\dot{n}_C^{\text{th}}$ . The last term, corresponding to diffusive proton escape, has the same form as in LZ87. The function  $f$  accounts for the effect of relativistic forward scattering, which reduces the amount of photon diffusion inside the source, and it is given by equation (21b) in LZ87.

We treat Coulomb losses in the same way as in CB90 (see also Dermer and Liang 1989 for a treatment of the Coulomb process). At relativistic energies  $\gamma \gg 1$  and nonrelativistic pair temperatures ( $\Theta \ll 1$ ), the Coulomb loss rate takes the form (e.g., Gould 1975)

$$\dot{\gamma}_{\text{Coul}} \approx -\frac{3}{2} \frac{c}{R} \tau_T^{\text{th}} \ln \frac{\gamma^{1/2}}{\epsilon_p}, \quad (5a)$$

where  $\epsilon_p$  is the dimensionless plasma frequency,

$$\epsilon_p = \left( \frac{3a_0 \tau_T^{\text{th}}}{2R} \right)^{1/2}, \quad (5b)$$

and  $a_0 = 5.29 \times 10^{-9} \text{ cm}$  is the Bohr radius. The factor  $\ln \epsilon_p^{-1}$  for  $\tau_T^{\text{th}} = 1$  equals 17.4 for  $R = 10^7 \text{ cm}$  and 25.4 for  $R = 10^{14} \text{ cm}$ . At higher temperatures, the Coulomb cooling rate  $\dot{\gamma}_{\text{Coul}}$  for energies  $\gamma \gg \Theta$  is reduced by a factor  $\approx 1/(2\Theta)$  (see CB90 and references therein) relative to equation (5a).

We can compare the magnitude of Compton and Coulomb losses of an electron with the Lorentz factor  $\gamma$ . In a photon-starved plasma,  $l_s \ll l_e$ , Coulomb losses dominate below a  $\gamma_{\text{cr}}$  given by

$$\gamma_{\text{cr}}^2 \approx 10 \frac{\tau_T^{\text{th}}}{l_e} \ln \epsilon_p^{-1}. \quad (6a)$$

At  $l_e \lesssim 10^2$ ,  $\tau_T^{\text{th}} \propto l_e$  (e.g., Svensson 1987), and

$$\gamma_{\text{cr}}^2 \sim \ln \epsilon_p^{-1}, \quad (6b)$$

and at  $l_e \gtrsim 10^2$ ,  $\tau_T^{\text{th}} \propto l_e^{1/2}$ , and

$$\gamma_{\text{cr}}^2 \approx (100/l_e)^{1/2} \ln \epsilon_p^{-1}. \quad (6c)$$

We define the pair yield as the ratio of the power injected in the form of pair rest mass by the creation of  $e^+e^-$  pairs to the power injected in the primary pairs (see Guilbert, Fabian, and Rees 1983; Svensson 1987; LZ87),

$$Y \equiv \frac{\int_1^{\gamma_{\max}} P d\gamma}{\int_{\gamma_{\min}}^{\gamma_{\max}} \gamma Q d\gamma}. \quad (7a)$$

One may define an analogous quantity,  $Y_Q$ , for the primary pairs which represents the fraction of their injected energy contained in pair rest mass. For power-law pair injection,  $Q(\gamma) = Q_0 \gamma^{-\Gamma}$  for  $\gamma_{\min} \leq \gamma \leq \gamma_{\max}$ , where  $Y_Q$  is

$$Y_Q = \frac{\int_{\gamma_{\min}}^{\gamma_{\max}} \gamma^{-\Gamma} d\gamma}{\int_{\gamma_{\min}}^{\gamma_{\max}} \gamma^{-\Gamma+1} d\gamma} \\ = \begin{cases} \frac{(\Gamma-2)(\gamma_{\min}^{1-\Gamma} - \gamma_{\max}^{1-\Gamma})}{(\Gamma-1)(\gamma_{\min}^{2-\Gamma} - \gamma_{\max}^{2-\Gamma})} & \Gamma \neq 2; \\ \frac{\gamma_{\min}^{-1} - \gamma_{\max}^{-1}}{\ln(\gamma_{\max}/\gamma_{\min})} & \Gamma = 2. \end{cases} \quad (7b)$$

The dimensionless luminosity  $l_{\text{ann}}^{\text{th}}$  in pair annihilation from thermal pairs is then related to both pair yields from the primary and secondary pairs,

$$l_{\text{ann}}^{\text{th}} = \frac{4\pi}{3} \frac{\sigma_T R^2}{c} \int_0^\infty \epsilon \dot{n}_A^{\text{th}}(\epsilon) d\epsilon = \gamma_{\text{th}}(Y + Y_Q)l_e, \quad (8)$$

where  $\gamma_{\text{th}}$  is the average Lorentz factor in the Maxwell-Boltzmann distribution,

$$\gamma_{\text{th}} = 3\Theta + \frac{K_1(1/\Theta)}{K_2(1/\Theta)}, \quad (9)$$

and  $K_n$  is the modified Bessel function of the second kind of order  $n$ .

We will also introduce here the dimensionless power in secondary pairs,

$$l_{\text{pair}} \equiv \frac{4\pi}{3} \frac{\sigma_T R^2}{c} \int_1^{\gamma_{\text{max}}} \gamma P(\gamma) d\gamma. \quad (10)$$

This power is not directly radiated, and it equals the fraction of the power in photons produced inside the source that is absorbed in photon-photon pair production. This quantity will be important for assessing the importance of the Coulomb process (see eqs. [17] and [19]).

The escape of thermal pairs is treated as in Zdziarski (1985) by the means of a phenomenological parameter  $\beta_{\text{esc}}$  defined as the ratio of the travel time across the source to the escape time scale. The escape rate (at  $N_+ = N_-$ ) is then

$$\dot{N}_{\text{esc}}^{\text{th}} = -2\beta_{\text{esc}}(c/R)N_+. \quad (11)$$

We neglect here escape of nonthermal pairs (see the paragraph after eq. [3] above), which can be important under some circumstances.

We determine the Thomson optical depth of the thermal pairs by balancing pair annihilation of thermal pairs with both thermal and nonthermal pairs and pair escape with pair production. Since the effect of annihilation with the nonthermal pairs is small in most cases, we neglect it in equations (12)–(13) below,

$$-2N_+ N_- \frac{3}{8}\sigma_T c g_A - 2N_+ \beta_{\text{esc}} c/R + \int_1^{\gamma_{\text{max}}} [Q(\gamma) + P(\gamma)] d\gamma \simeq 0. \quad (12)$$

Here  $g_A(\Theta)$  is the relativistic correction to the thermal pair annihilation rate (eq. [68] of Svensson 1982). Since  $N_+ = N_-$  for pure pair injection, equation (12) yields an estimate of the Thomson optical depth of the thermal pairs as

$$\tau_T^{\text{th}} \simeq \left[ \left( \frac{8\beta_{\text{esc}}}{3g_A} \right)^2 + \frac{4}{\pi g_A} (Y + Y_Q)l_e \right]^{1/2} - \frac{8\beta_{\text{esc}}}{3g_A}. \quad (13)$$

(The effect of nonthermal pair annihilation on pair equilibrium is included in our numerical treatment.) The pair escape term in equation (12) becomes equal to the pair annihilation term when  $\tau_T^{\text{th}} = 8\beta_{\text{esc}}/3g_A$ . Pair escape is then negligible at  $\tau_T^{\text{th}}$  larger than that value. Using the linear dependence between the pair yield and compactness at low  $l_e$  (e.g., Svensson 1987), and using equation (13), we find that pair escape is negligible compared to the pair annihilation at

$$l_e \gtrsim 10^2 \beta_{\text{esc}}. \quad (14)$$

The thermal pairs are produced by thermalization of both the primary and secondary pairs and removed by pair annihi-

lation and escape from the source. They cool and heat through Compton interactions with the photon field  $n(\epsilon)$  and through Coulomb interactions with the nonthermal electrons, and they cool via thermal bremsstrahlung. The energy balance equation for the thermal pairs is thus

$$-\int_0^\infty \dot{n}_C^{\text{th}} \epsilon d\epsilon - \int_0^\infty \dot{n}_B^{\text{th}} \epsilon d\epsilon - \int_0^\infty \dot{n}_A^{\text{th, nth}} \epsilon d\epsilon + \gamma_{\text{th}} \dot{N}_{\text{esc}}^{\text{th}} + \gamma_{\text{th}} \int_1^{\gamma_{\text{max}}} (P + Q) d\gamma - \int_1^{\gamma_{\text{max}}} \dot{\gamma}_{\text{Coul}} N d\gamma = 0. \quad (15)$$

A negative term in equation (15) corresponds to removal and a positive one corresponds to production of thermal energy, respectively. The factor  $\dot{n}_A^{\text{th, nth}}$  includes annihilation of thermal pairs with both thermal and nonthermal pairs. The integral over  $\dot{n}_A^{\text{th, nth}}$  gives the rate at which annihilation removes energy from a unit volume of the source, i.e., the integrated annihilation emissivity, and thus the annihilation compactness (see eq. [9]). We use the fit given by Svensson (1982, eq. [70]) for the integrated thermal annihilation emissivity.

The term  $\gamma_{\text{th}} \int (P + Q) d\gamma$  gives the rate at which energy is injected into the emission region in the form of nonthermal pairs that cool and become thermal. Since the probability of annihilation increases with decreasing energy, pairs with energies lower than  $\gamma_{\text{th}}$  predominantly annihilate. Thus the sum of the third, fourth, and fifth terms in equation (15) is positive, and annihilation *heats* the thermal plasma. The heating rate due to annihilation can be comparable to the cooling rate due to bremsstrahlung, the second term in equation (15); for example, both rates are approximately equal at  $\Theta = 1$ .

The thermal pairs upscatter and downscatter photons present in the source. Low-energy photons are predominantly upscattered repeatedly by the thermal pairs. The Compton parameter  $y$  is a convenient measure of the efficiency of the thermal upscattering, with  $\epsilon_f = e^y \epsilon_i$ , where the indices  $i$  and  $f$  indicate photon before and after scattering, respectively, and  $\epsilon_f < \Theta$ . The nonrelativistic form of the parameter is given, e.g., by equation (7.41a) in Rybicki and Lightman (1979). An approximate general expression valid at any temperature is

$$y \simeq \ln(1 + 4\Theta + 16\Theta^2) \tau_T^{\text{th}} \left( 1 + \frac{\tau_T^{\text{th}}}{3} \right), \quad (16)$$

which reduces to the nonrelativistic form at  $\Theta \ll 1$ . (Note that eq. [7.41b] in Rybicki and Lightman 1979 for the extreme relativistic Compton parameter appears to have no physical interpretation and is inconsistent with the definition of  $y$  by the relation  $\epsilon_f = e^y \epsilon_i$ .)

In our numerical treatment, we assume that the injected nonthermal pairs cool until they reach energy  $\gamma_{\text{th/nth}} = 1 + 4\Theta$ , at which point they are transferred (along with their energy) to the thermal pair distribution. The results do not depend sensitively on the exact value of the numerical constant in front of the factor  $\Theta$ .

For low temperatures ( $\Theta \lesssim 0.1$ ),  $\dot{\gamma}_{\text{Coul}}$  is roughly constant over a wide range of pair energies (see eq. [5]). We can obtain an order-of-magnitude estimate of the dimensionless Coulomb cooling rate of the nonthermal pairs (above  $\gamma_{\text{th/nth}}$ ),  $l_{\text{Coul}}$ , by bringing  $\dot{\gamma}_{\text{Coul}}$  outside the integrand and evaluating the integral at  $\gamma = 1$ ,

$$l_{\text{Coul}} \equiv -\frac{4\pi}{3} \frac{\sigma_T R^2}{c} \int_{\gamma_{\text{th/nth}}}^{\gamma_{\text{max}}} \dot{\gamma}_{\text{Coul}} N(\gamma) d\gamma \quad (17a)$$

$$\simeq 2\pi \tau_T^{\text{th}} \tau_T^{\text{nth}} \ln \epsilon_p^{-1}, \quad (17b)$$

where equation (17a) defines  $l_{\text{Coul}}$ , and  $\tau_{\text{T}}^{\text{nth}}$  is the Thomson optical depth of the nonthermal electrons and positrons,

$$\tau_{\text{T}}^{\text{nth}} = \sigma_{\text{T}} R \int_{\gamma_{\text{th/nth}}}^{\gamma_{\text{max}}} N(\gamma) d\gamma. \quad (18)$$

The energy input from the Coulomb process to the thermal pairs (the last term in eq. [15]) also includes the contribution from nonthermal pairs with  $\gamma < \gamma_{\text{th/nth}}$ . Assuming the nonthermal pairs with  $\gamma < \gamma_{\text{th/nth}}$  thermalize immediately (via Coulomb scattering), the additional energy input is given by

$$\frac{4\pi \sigma_{\text{T}} R^2}{3c} \left[ \int_1^{\gamma_{\text{th/nth}}} \gamma(Q+P) d\gamma + \gamma_{\text{th/nth}} \times \int_{\gamma_{\text{th/nth}}}^{\gamma_{\text{max}}} (Q+P) d\gamma - \gamma_{\text{th}} \int_1^{\gamma_{\text{max}}} (Q+P) d\gamma \right]. \quad (19)$$

Note that the term of equation (19) can in principle be either negative or positive, depending on the form of  $P+Q$ . In all numerical cases we have considered (see § III), the term of equation (19) is positive and much less than  $l_{\text{Coul}}$  of equation (17a).

To assess the relative importance of Coulomb heating of the thermal distribution, one should use the quantity  $l_{\text{Coul}}/l_e$ . This quantity gives the fraction of the injected power that is transferred to the thermal distribution through Coulomb interactions. On the other hand, the relative importance of Coulomb cooling pairs of the nonthermal distribution is determined by the fraction of the nonthermal power in both the primary and secondary pairs that is transferred via Coulomb interactions to the thermal component, which is approximately given by  $l_{\text{Coul}}/(l_e + l_{\text{pair}})$ . (The  $l_{\text{pair}}$  is defined by eq. [10], and Table 1 in § III lists the values of  $l_{\text{Coul}}/l_e$  and  $l_{\text{pair}}/l_e$ .)

Thermal bremsstrahlung in a pair plasma has contributions from  $e^{\pm}e^{\pm}$  and  $e^+e^-$  interactions. The nonthermal electrons emit bremsstrahlung while interacting with the thermal plasma and with themselves. Since  $\tau_{\text{T}}^{\text{th}} \gg \tau_{\text{T}}^{\text{nth}}$ , the latter contribution is much less than the former. We treat bremsstrahlung in the way

described in CB90. The Appendix describes a simple treatment of nonthermal bremsstrahlung at  $\gamma \gg 1$ .

The thermal bremsstrahlung self-absorption frequency  $\epsilon_{\text{sa}}$ , defined by  $\tau_{\text{sa}}(\epsilon_{\text{sa}}) = 1$ , can be written as

$$\epsilon_{\text{sa}} = \tau_{\text{T}}^{\text{th}} \left\{ \frac{3\pi a_0}{8} \frac{1}{R} \frac{1}{\Theta} \left[ \frac{\epsilon \dot{n}_{\text{B}} \sigma_{\text{T}} R^2}{(\tau_{\text{T}}^{\text{th}})^2 c \alpha_{\text{f}}} \right] \right\}^{1/2}, \quad (20)$$

where  $\alpha_{\text{f}}$  is the fine-structure constant. The dimensionless factor in brackets is a function of  $\epsilon$  and  $\Theta$  only and is of the order of unity at mildly relativistic temperatures. For  $R = 10^7$  cm,  $\epsilon_{\text{sa}} \sim 10^{-8}$ . Since the self-absorbed part of the spectrum contains very little energy compared to the optically thin part, we assume  $\dot{n}_{\text{B}} = 0$  below  $\epsilon_{\text{sa}}$ . Self-absorption by nonthermal electrons can be neglected compared to that by the thermal ones (see Appendix).

### III. RESULTS

In this section, our numerical results are discussed and interpreted. We will discuss mostly those features in the spectra that are specific to photon-deficient plasmas. We refer the reader to LZ87 for discussion of spectra from nonthermal pair equilibrium plasmas with abundant soft photons.

We consider power-law pair injection,  $Q(\gamma) = Q_0 \gamma^{-\Gamma}$  for  $\gamma_{\text{min}} \leq \gamma \leq \gamma_{\text{max}}$ . The dimensionless parameters that specify a model are  $l_e$ ,  $l_s$ ,  $\Theta_{\text{bb}}$ ,  $\Gamma$ ,  $\gamma_{\text{min}}$ ,  $\gamma_{\text{max}}$ , and  $\beta_{\text{esc}}$ . In most models, we set  $\beta_{\text{esc}} = 0$ . There is also a weak dependence on  $R$  through the Coulomb cooling rate (eqs. [5]–[6]) and the bremsstrahlung self-absorption energy (eq. [20]). We assume  $R = 10^{14}$  cm and  $\epsilon_{\text{sa}} = 10^{-9}$ .

The main input and output quantities for the models presented in this section are given in Table 1. The quantities  $y$ ,  $\tau_{\text{T}}^{\text{th}}$ ,  $l_{\text{Coul}}$ , and  $l_{\text{pair}}$  are defined in equations (16), (18), (17a), and (10), respectively. The quantities  $l_{2-10}$  and  $\alpha_{2-10}$  are the 2–10 keV compactness and average energy spectral index, respectively. The dimensionless energy  $\epsilon_{*}$  corresponds to  $\tau_{\gamma\gamma}(\epsilon_{*}) = 1$ . The model numbers in Table 1 correspond to the cases pre-

TABLE 1  
RESULTS FOR THE PRESENTED MODELS

Model	$l_e$	$l_s/l_e$	$\gamma_{\text{max}}$	$\Gamma$	$\Theta_{\text{bb}}$	$\Theta$	$\tau_{\text{T}}^{\text{th}}$	$\tau_{\text{T}}^{\text{nth}}$	$y$	$Y$	$l_{\text{Coul}}/l_e$	$l_{\text{pair}}/l_e$	$\alpha_{2-10}$	$l_{2-10}/l_e$	$\epsilon_{*}$
1ai, 2i	1	0	$10^3$	2.5	...	0.91	0.94	0.0078	3.6	0.0069	0.34	0.017	0.06	0.0031	$>10^3$
1aii, 6ii	1	$10^{-2}$	$10^3$	2.5	$10^{-4}$	0.51	0.73	0.0069	1.8	0.0056	0.34	0.016	0.51	0.030	$>10^3$
1aiii	1	1	$10^3$	2.5	$10^{-4}$	0.098	0.56	0.0051	0.29	0.0015	0.37	0.006	1.36	0.13	400
1bi	$10^3$	0	$10^3$	2.5	...	0.081	25	0.10	83	0.25	0.31	0.67	-0.21	0.0017	1
1bii	$10^3$	$10^{-2}$	$10^3$	2.5	$10^{-4}$	0.016	20	0.033	10	0.090	0.12	0.32	-0.44	0.11	1
1biii	$10^3$	1	$10^3$	2.5	$10^{-4}$	0.0011	18	0.011	0.56	0.025	0.044	0.089	2.11	0.26	1
1ci	30	0	$10^3$	2.5	...	0.30	4.7	0.037	16	0.19	0.48	0.36	0.00	0.0027	3
1cii, 7i	30	$10^{-2}$	$10^3$	2.5	$10^{-4}$	0.11	3.4	0.032	3.6	0.048	0.45	0.17	0.36	0.047	5
1ciii	30	1	$10^3$	2.5	$10^{-4}$	0.012	3.0	0.013	0.29	0.011	0.24	0.049	1.06	0.18	11
3i	30	0	$10^3$	1.5	...	0.52	3.6	0.055	17	0.16	0.55	0.55	-0.02	0.046	6
3ii	30	$10^{-2}$	$10^3$	1.5	$10^{-4}$	0.15	3.3	0.037	4.7	0.10	0.35	0.78	0.42	0.039	5
3iii	30	1	$10^3$	1.5	$10^{-4}$	0.016	1.7	0.0087	0.18	0.054	0.090	0.44	0.70	0.10	9
4i	$10^2$	$10^{-3}$	$10^3$	1	$10^{-4}$	0.16	6.0	0.082	13	0.24	0.56	1.49	0.06	0.0061	2
4ii	$10^2$	$10^{-3}$	$10^3$	2	$10^{-4}$	0.15	6.4	0.074	14	0.19	0.54	0.77	0.05	0.0066	2
4iii	$10^2$	$10^{-3}$	$10^3$	3	$10^{-4}$	0.11	7.6	0.053	13	0.087	0.54	0.17	0.04	0.0077	2
5i	$10^2$	$10^{-2}$	10	2.5	$10^{-3}$	0.11	7.4	0.053	13	0.067	0.45	0.097	0.06	0.010	2
5ii	$10^2$	$10^{-2}$	$10^2$	2.5	$10^{-3}$	0.12	7.0	0.060	13	0.11	0.49	0.24	0.07	0.0095	2
5iii	$10^2$	$10^{-2}$	$10^3$	2.5	$10^{-3}$	0.12	6.9	0.062	12	0.12	0.50	0.35	0.08	0.0094	2
6i	1	$10^{-2}$	$10^3$	2.5	$10^{-4}$	0.88	0.18	0.027	0.54	0.00034	0.20	0.002	0.58	0.015	$>10^3$
7ii	30	$10^{-2}$	$10^3$	2.5	$10^{-4}$	0.14	2.5	0.044	3.0	0.072	0.44	0.29	0.38	0.043	5
7iii	30	$10^{-2}$	$10^3$	2.5	$10^{-4}$	0.15	2.3	0.042	2.8	0.090	0.39	0.39	0.40	0.040	5

NOTES.— $\gamma_{\text{min}} = 1.6$ ,  $R = 10^{14}$  cm,  $\epsilon_{\text{sa}} = 10^{-9}$ ,  $\beta_{\text{esc}} = 0$  in all models except model 6i, where  $\beta_{\text{esc}} = 0.3$  and the luminosity emitted in escaping photons  $l_{\text{em}} = 0.31$ ; model 7ii, where  $\gamma_{\text{min}} = 5$ ; and model 7iii, where  $\gamma_{\text{min}} = 10$ .

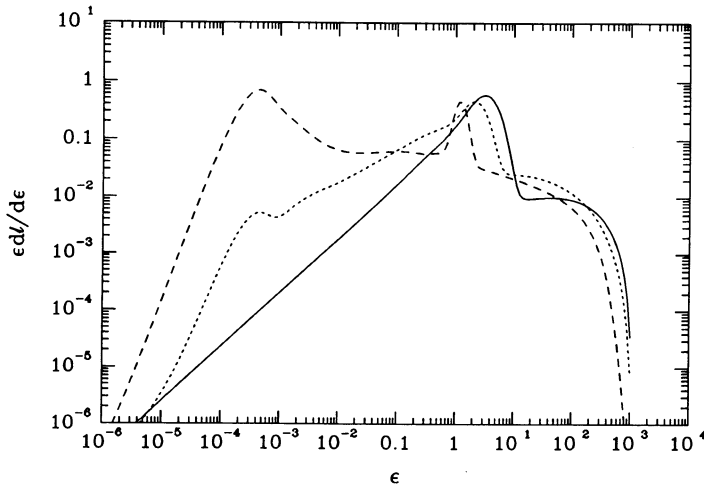


FIG. 1a

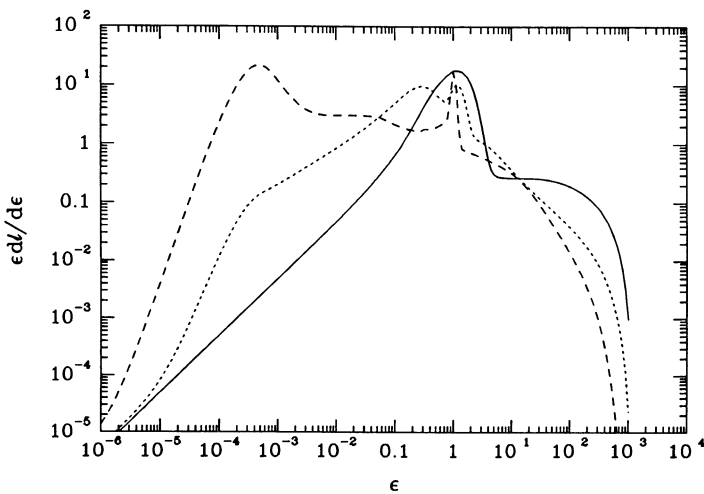


FIG. 1c

FIG. 1.—Effect of varying external soft photon injection for steep pair injection,  $\Gamma = 2.5$ . Solid curves have no external soft photon injection, i.e., all photons come from bremsstrahlung. Dotted curves have  $l_s = 10^{-2}l_e$ , while dashed curves have  $l_s = l_e$ . Models in (a) have  $l_e = 1$ ; models in (b) have  $l_e = 10^3$ ; models in (c) have  $l_e = 30$ . The other input and output model parameters are given in Table 1 (models 1a, b, c; i, ii, iii).

sented in Figures 1–7 below, and i, ii, iii correspond to the solid, dotted, and dashed curves, respectively.

Figures 1a–1c present spectra from sources with power-law electrons injected with the index  $\Gamma = 2.5$ . The compactnesses in the pair injection are (a)  $l_e = 1$ , (b)  $l_e = 10^3$ , and (c)  $l_e = 30$ . Solid curves in Figures 1a–1c correspond to the only source of photons being bremsstrahlung. Bremsstrahlung radiation is emitted by both the thermal and nonthermal pairs. The dotted and dashed curves correspond to the addition of blackbody sources of soft photons with  $l_s = 10^{-2}l_e$  and  $l_s = l_e$ , respectively.

At  $l_e = 1$  and  $l_s = 0$  (solid curve in Fig. 1a), the equilibrium temperature is relativistic,  $\Theta \simeq 0.9$  since un-Comptonized non-relativistic bremsstrahlung would radiate only  $l \ll 1$  (e.g., Svensson 1986). There is little production of secondary pairs. The equilibrium Thomson optical depth of the thermal pairs is relatively small,  $\tau_T^{\text{th}} \simeq 0.9$ , and is due mostly to cooled primary pairs. The spectrum consists of three components: thermal

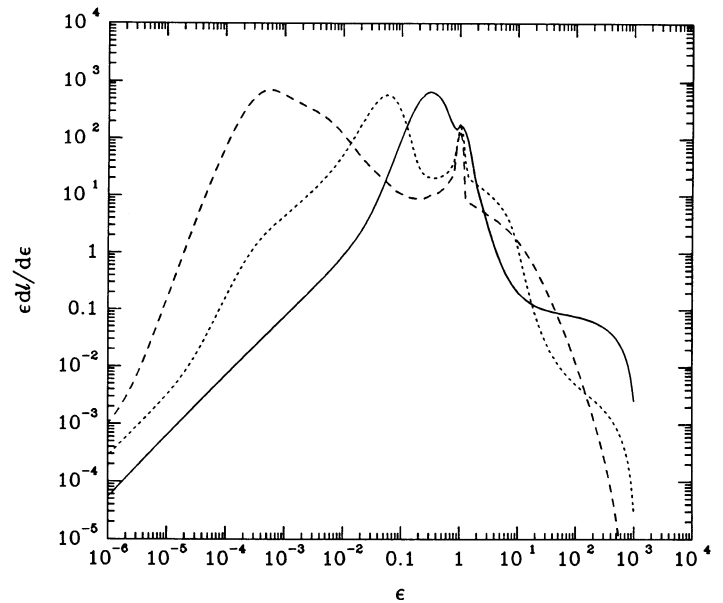


FIG. 1b

bremsstrahlung, exponentially cutoff at  $\epsilon > \Theta$ ; a pair annihilation spectrum (mostly thermal) peaked at  $\epsilon \sim 1 + (3/2 - 3)\Theta$ , (the factor in parentheses times  $\Theta$  represents the average thermal kinetic energy); and nonthermal bremsstrahlung, extending up to  $\epsilon \sim \gamma_{\text{max}}$ . The bremsstrahlung components are shown in Figure 2. Comptonization has a relatively minor effect on the spectrum. The X-ray spectral index of  $\alpha_x \sim 0$  is typical for bremsstrahlung. The optical depth of the nonthermal electrons is  $\tau_T^{\text{nth}} \simeq 10^{-2} \ll 1$ , and the amplitude of the nonthermal bremsstrahlung is much less than that of the thermal one. The thermal electrons are heated by both Compton and Coulomb interactions. Coulomb interactions dominate and transfer about one-third the injected power to the thermal electrons.

The dotted curve in Figure 1a gives the spectrum corresponding to an additional source of blackbody photons at  $\Theta_{\text{bb}} = 10^{-4}$  with a compactness,  $l_s$ , one-hundredth the electron compactness,  $l_e$ . The  $\epsilon \lesssim 1$  spectrum is dominated by the blackbody photons singly scattered by the nonthermal pairs and repeatedly Compton upscattered by the thermal pairs. The

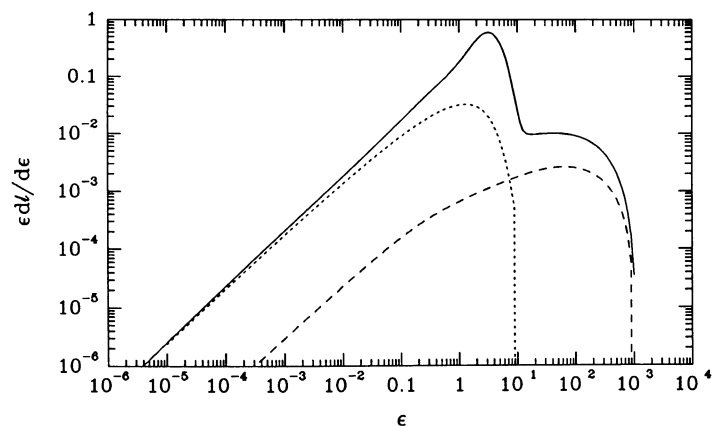


FIG. 2.—Thermal (dotted curve) and nonthermal (dashed curve) bremsstrahlung contribution to the spectrum of the solid curve in Fig. 1a.

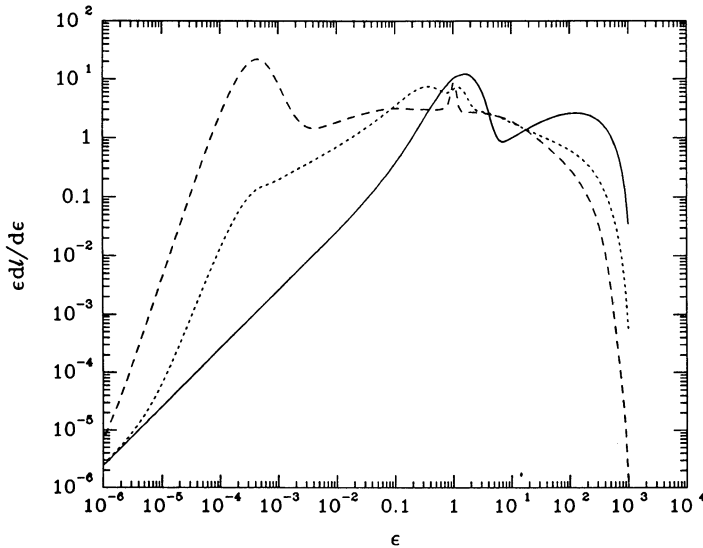


FIG. 3.—The effect of varying external soft photon injection for flat pair injection,  $\Gamma = 1.5$ . Solid, dotted, and dashed curves correspond to  $l_s/l_e = 0$ ,  $10^{-2}$ , and 1, respectively. Input and output parameters are given in Table 1 (models 3i, 3ii, 3iii).

2–10 keV spectral index is  $\alpha_{2-10} \simeq 0.5$ . The equilibrium temperature is now lower,  $\Theta \simeq 0.5$ . There is an annihilation feature, which is mostly due to annihilation of pairs from the primary injection,  $Q$ , after they have thermalized. At  $\epsilon \gg 1$ , the spectrum consists of both nonthermal bremsstrahlung emission and upscattered blackbody and X-ray power-law photons.

Spectra with parameters similar to those corresponding to the dotted curve were discussed by ZL86. They predicted the spectra to be of the broken power-law form with an  $\alpha_x < 1$  power-law joining onto a steeper  $\alpha_\gamma > 1$  power-law at  $\epsilon \sim 1$ . In contrast, our results give a sharp drop of a factor of  $\sim 10$  in the spectrum beyond the annihilation spectrum. The amplitude of the  $\gamma$ -ray power-law is reduced by that factor. This is due to the effect of efficient Coulomb cooling ( $l_{\text{Coul}} \simeq 0.3l_e$ ) that affects

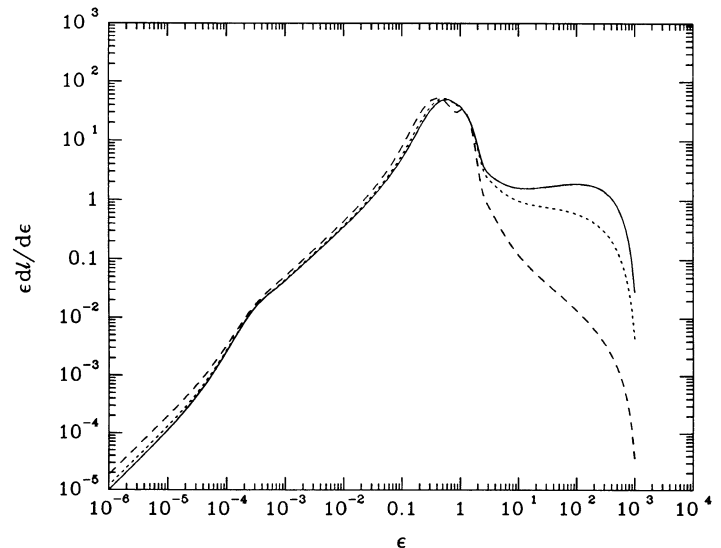


FIG. 4.—The effect of varying  $\Gamma$  in an  $l_s = 10^{-3}l_e$  case. Solid, dotted, and dashed curves correspond to  $\tau = 1, 2, 3$ , respectively. See Table 1 (models 4i, 4ii, 4iii) for the parameters.

mostly mildly relativistic nonthermal electrons and reduces their Thomson optical depths to  $\tau_T^{\text{nth}} \ll 1$ .

The dashed curve corresponds to a large amplitude of the blackbody photons,  $l_s = l_e$ . The resulting spectrum is a “classical” one, with an X-ray and  $\gamma$ -ray power-law corresponding to the first-order Compton upscattering of the blackbody photons by the thermal component, directly following the blackbody spectrum. There is a distinct annihilation feature due to annihilation of the pairs of the primary injection ( $Q$ ).

Figure 1b shows three cases with the same ratios  $l_s/l_e$ , but with a large  $l_e = 10^3$ . The equilibrium optical depths of the thermal pairs are large, which has rather dramatic effects on the spectra. The equilibrium temperatures are now much smaller due to the effect of large  $\tau_T^{\text{th}}$ . (A large  $\tau_T^{\text{th}}$  causes a

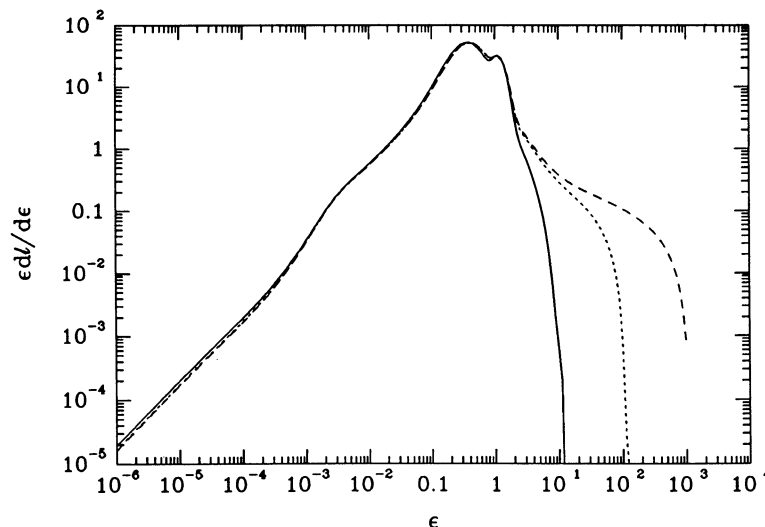


FIG. 5.—The effect of varying  $\gamma_{\text{max}}$  in an  $l_s = 10^{-2}l_e$  case. Solid, dotted, and dashed curves correspond to  $\gamma_{\text{max}} = 10, 10^2, 10^3$ , respectively. See Table 1 (models 5i, 5ii, 5iii) for the parameters.

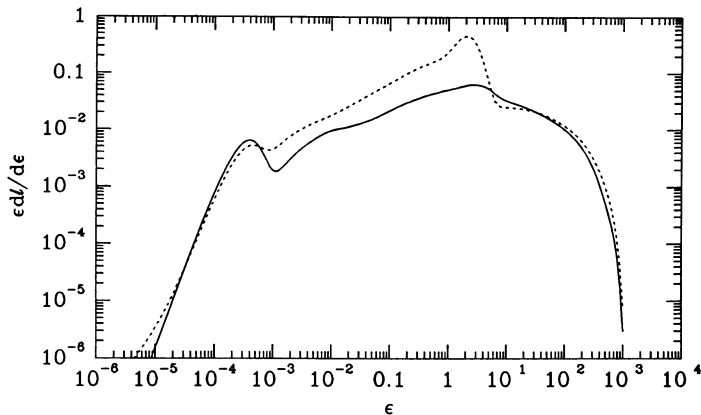


FIG. 6.—The effect of pair escape in a low-compactness,  $l_e = 1$ , case. The solid curve corresponds to escape of thermal pairs with  $\beta_{\text{esc}} = 0.3$ , whereas the dotted curve is for the same parameters but  $\beta_{\text{esc}} = 0$ . See Table 1 (models 6i, 1aii) for the parameters.

diffusive enhancement of the density of soft photons as well as a softening of their distribution, and thus it increases the cooling rate of pairs.) The solid curve corresponding to  $l_s = 0$  gives heavily thermally Comptonized bremsstrahlung spectrum with a Wien peak at  $\epsilon \sim 3\Theta \simeq 0.2$ . The Wien peak is followed by an annihilation feature and a low-amplitude non-thermal bremsstrahlung spectrum. When some blackbody photons are added to the source (*dotted curve*), the equilibrium temperature decreases and the Wien peak shifts to lower energies. It is now followed by a dip due to Compton down-scattering by the thermal electrons. Note that those spectra also differ from those of ZL86, mostly due to the effect of thermal Comptonization, which was not included in that analysis. When  $l_s = l_e$  (*dashed curve*), the Wien peak disappears and there is a nonthermal X-ray power law followed by the downscattering dip (see, e.g., LZ87).

Figure 1c shows cases intermediate between those of Figures 1a and 1b, with an electron compactness of  $l_e = 30$ . The Wien peak in the solid curve ( $l_s = 0$ ) coincides with the annihilation feature. The Wien peak at  $l_s = 0.01l_e$  (*dotted curve*) and the

downscattering dip at  $l_s = l_e$  (*dashed curve*) are much weaker than at  $l_e = 10^3$ .

Note that the dotted spectrum is approximately a broken power law, with a break around 100 keV ( $\epsilon \simeq 0.2$ ). There is a weak annihilation feature superposed on the  $\gamma$ -ray power law. This spectrum resembles some  $\gamma$ -ray burst spectra (see § IV and, e.g., Figs. 1a, 1b in Zdziarski 1987).

Figure 3 shows the same cases as Figure 1c, but with  $\Gamma = 1.5$ . The changed  $\Gamma$  has little effect on the  $\epsilon \lesssim 1$  spectra at  $l_s = 0$  (*solid curve*) and  $l_s = 0.01l_e$  (*dotted curve*), with repeated Compton scattering by thermal pairs dominating. In this case, the  $\epsilon \gtrsim 1$  spectra are much harder than for  $\Gamma = 2.5$ , reflecting the hardened distributions of the injected nonthermal electrons. Again, the  $l_s = 0.01l_e$  spectrum resembles the classical  $\gamma$ -ray burst spectra (see § IV). The  $l_s = l_e$  spectrum is dominated by the first-order Compton scattering by nonthermal electrons (see, e.g., LZ87).

Figure 4 shows the effect of changing  $\Gamma$  in an  $l_s \ll l_e$  case. The spectrum up to the annihilation peak remains unaffected, since it is mostly thermal. Only the shape of the high-energy  $\gamma$ -ray spectrum changes. It becomes steeper and of lower amplitude as  $\Gamma$  increases. Changing  $\Gamma$  in the  $l_s = l_e$  case has a much more pronounced effect, as can be seen in Figures 1c and 3 above, and in, e.g., LZ87. In that case, the overall slope of the spectrum steepens with increasing  $\gamma$  (see, e.g., LZ87). The downscattering dip becomes more pronounced with increasing  $\Gamma$ , since  $\tau_1^{\text{th}}$  increases as well.

Figure 5 shows the effect of changing  $\gamma_{\text{max}}$  at  $l_s = 0.01l_e$  and  $l_e = 100$ . The  $\epsilon \lesssim 1$  spectrum remains unchanged with changing  $\gamma_{\text{max}}$ , which is a consequence of the dominance of the thermal component. Only the cutoff in the  $\gamma$ -ray spectrum moves, with  $\epsilon_{\text{max}} \simeq \gamma_{\text{max}}$ .

Figure 6 shows the effect of escape of thermal pairs at low compactness,  $l_e = 1$ , and  $l_s \ll l_e$ . The equilibrium optical depth of the thermal pairs is reduced by a large factor, since escape is a faster process than pair annihilation. Since the escaping pairs carry away a large fraction of the injected energy, in both kinetic and rest mass form, the luminosity in photons is reduced by a factor of a few. At larger compactnesses, pair

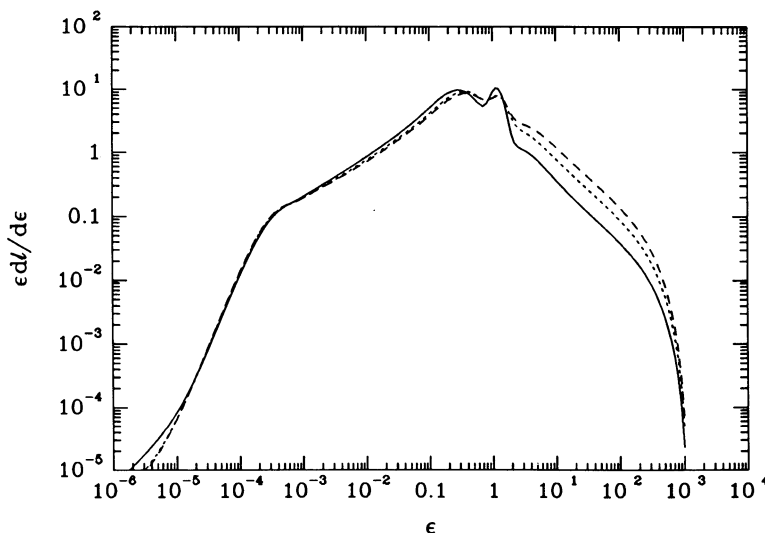


FIG. 7.—The effect of varying  $\gamma_{\text{min}}$  in an  $l_s = 10^{-2}l_e$  case. Solid, dotted, and dashed curves correspond to  $\gamma_{\text{min}} = 1.6, 5, 10$ , respectively. See Table 1 (models 1cii, 7ii, 7iii) for the parameters.

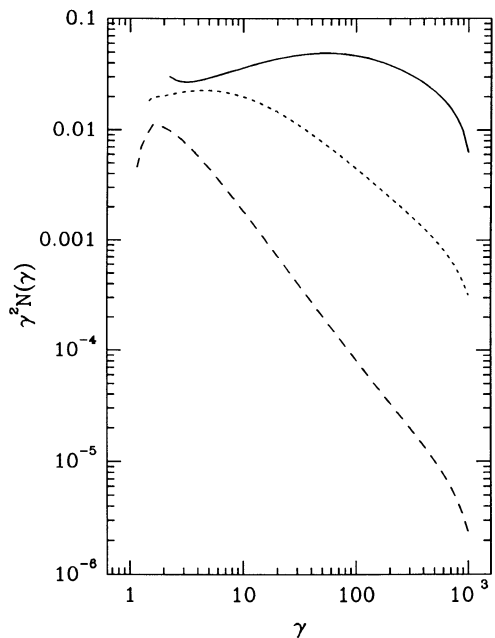


FIG. 8.—Steady state pair distributions corresponding to the photon spectra shown in Fig. 1c.

escape has no effect, since then pair annihilation is faster (see eq. [14]).

Figure 7 shows the effect of changing the value of the low-energy cutoff,  $\gamma_{\min}$ , in the injected distribution in the case of step injection,  $\gamma = 2.5$ . Since an increase of  $\gamma_{\min}$  at constant  $l_e$  gives more nonthermal pairs at high energies, the amplitude of

the  $\gamma$ -ray spectrum increases as well. In addition, the total number of injected pairs decreases with increasing  $\gamma_{\min}$ , which causes a reduction in the equilibrium Thomson optical depth of the thermal plasma and a corresponding reduction in the cooling rate of the nonthermal electrons. Note that at  $\gamma_{\min} = 5-10$  the spectrum is of an approximate broken power-law form, similar to the spectra of classical  $\gamma$ -ray bursts (see § V). (In models with the first-order Compton scattering dominating,  $l_s \gtrsim l_e$ , changing  $\gamma_{\min}$  results in a changing break in the spectrum at  $\sim \gamma_{\min}^2 \Theta$ ).

Figure 8 shows examples of the steady state nonthermal pair distributions. The distributions correspond to the photon spectra shown in Figure 1c, with  $l_e = 30$ . The distributions are cut off at  $\gamma_{\text{th/nth}}$ , as discussed in § II. The distributions in the two photon-starved cases (solid and dotted line, with  $l_s/l_e = 0$  and  $10^{-2}$ , respectively) have slopes approximately given by  $p \simeq \Gamma + \alpha_x$ , where  $N(\gamma) \propto \gamma^{-p}$  and  $\alpha_x$  is the X-ray power-law index. This is due to electron cooling dominated by the upscattered X-ray and UV photons; see, e.g., ZL86. Note that most of the scatterings are in the Thomson ( $\epsilon\gamma \lesssim 1$ ) regime. The dashed line corresponds to the case with abundant soft photons, in which  $p \simeq \Gamma + 1$  (see, e.g., Blumenthal and Gould 1970).

Finally, Figure 9 plots some of the dependences of the source parameters  $\Theta$ ,  $\tau_T^{\text{th}}$ ,  $\tau_T^{\text{nth}}$ ,  $\gamma$ ,  $Y$ , and  $l_{\text{Coul}}/l_e$  on the soft photon ratio,  $l_s/l_e$ , for the input parameters corresponding to Figures 1c and 8 ( $l_e = 30$ ,  $\gamma = 2.5$ ,  $\gamma_{\min} = 1.6$ ). The plasma temperature (*crosses*) and the Compton parameter (*open circles*) decline quickly with increasing  $l_s/l_e$  due to increasing cooling on the soft photons. A corresponding decline in the pair yield (*filled circles*) is due to the general softening of the spectrum with much fewer photons above the threshold for pair production for large  $l_s/l_e$  (see Fig. 1c). The thermal optical depth

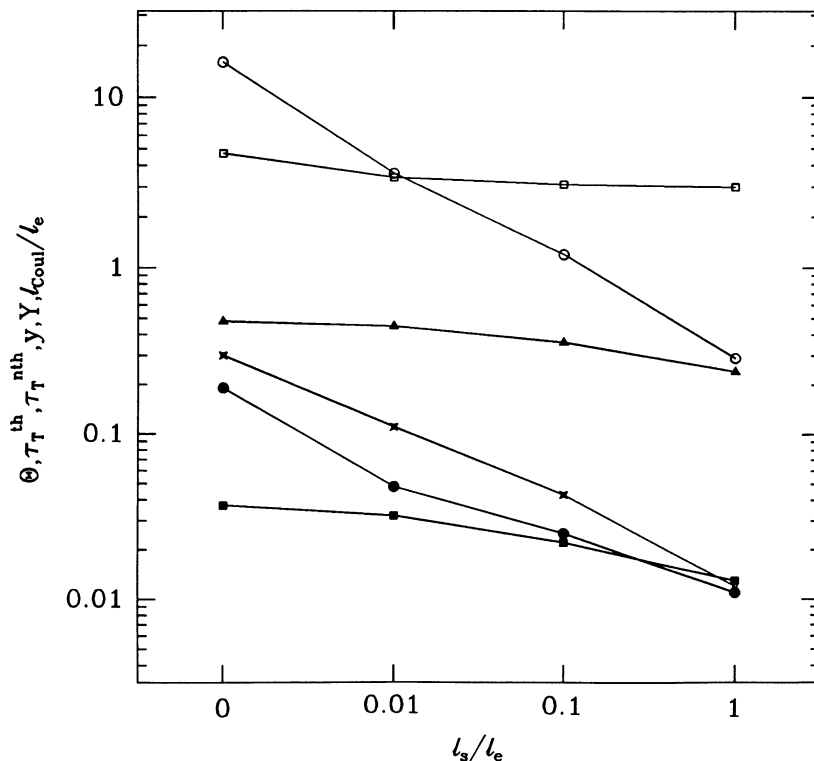


FIG. 9.—Dependence of  $\Theta$  (*crosses*),  $\tau_T^{\text{th}}$  (*open squares*),  $\tau_T^{\text{nth}}$  (*filled squares*), the Compton parameter  $\gamma$  (*open circles*), the pair yield  $Y$  (*filled circles*), and  $l_{\text{Coul}}/l_e$  (*triangles*) on  $l_s/l_e$  for  $l_e = 30$ . Other plasma parameters correspond to the cases given in Figures 1c and 8.

(*open squares*) is almost constant, as the bulk of thermal pairs are primary ones from the steep primary injection with low  $\gamma_{\min}$  (see eqs. [8] and [13]). The low value of  $\gamma_{\min}$  and  $\Gamma > 2$  is also responsible for the relatively large  $l_{\text{Coul}}/l_e$  (*triangles*) even at  $l_s/l_e = 1$ . Most of the nonthermal power is injected at  $\gamma_{\min} = 1.6$ , where the Coulomb losses are large compared to the Compton ones. Effective Compton and Coulomb cooling is responsible for the low values of  $\tau_T^{\text{th}}$  (*filled squares*).

Analysis of the values of  $l_{\text{Coul}}/l_e$  and  $l_{\text{pair}}/l_e$  in Table 1 shows that Coulomb process is important for heating the thermal pairs and cooling nonthermal ones in a wide range of parameters. (The relative importance of Coulomb heating of the thermal distribution is given by  $l_{\text{Coul}}/l_e$ , and the importance of Coulomb cooling of the nonthermal distribution is given by  $l_{\text{Coul}}/(l_e + l_{\text{pair}})$ ; see § III). The Coulomb process is always important when  $l_s/l_e \ll 1$ , even at large  $l_e$ , although the values of  $l_{\text{Coul}}/l_e$  and  $l_{\text{Coul}}/(l_e + l_{\text{pair}})$  diminish with increasing  $l_e$ . Coulomb interactions are negligible in most cases for  $l_s/l_e \gtrsim 1$  (see eq. [6]). The case when it is important for  $l_s/l_e = 1$  is for low  $l_e$  and  $\Gamma > 2$  (model 1aiii).

#### IV. DISCUSSION AND CONCLUSIONS

We have studied relativistic plasmas where energy is supplied in the form of relativistic nonthermal electron-positron pairs and soft photons. The plasma in steady state consists of the thermalized pairs and the nonthermal pairs in the process of cooling. We have considered situations where the power injected in the soft photons is much less than that in the relativistic pairs, i.e., photon-starved plasmas. Our main conclusions can be summarized as follows.

1. The overall form of the spectra from nonthermal pair-starved plasmas consists of: a rising ( $\nu F_\nu$ ) spectrum at low energies with  $\alpha_x \sim 0$ , a single or double peak in the 0.1–1 MeV energy range, a cutoff above the peak, and a  $\gamma$ -ray tail with a varying slope depending on the plasma parameters.

2. The low-energy power-law is mostly due to the primary soft photons being repeatedly upscattered by the hot thermal electrons. The equilibrium temperature of the thermal electrons we have found is in the  $\Theta \simeq 0.02$ –1 (10 keV to 0.5 MeV) range (see Table 1 except the photon abundant  $l_s/l_e = 1$  cases). The temperature increases with decreasing  $l_e$  and  $l_s/l_e$ . The relatively narrow range of temperature is due to the efficiency of Comptonization increasing greatly at relativistic energies (see, e.g., Rybicki and Lightman 1979) and the rapid increase of the pair production rate at relativistic temperatures (pair thermostat; see, e.g., Svensson 1984). The Comptonization parameter  $\gamma$  is greater than 1 (see Table 1), which results in hard spectra followed by Wien peaks. This peak is either followed or amplified by the one due to annihilation photons, at 0.5–1 MeV photon energies. The low-energy power-laws followed by the Wien peaks have largely thermal character and resemble those from thermal plasmas in pair equilibrium (see, e.g., Zdziarski 1984, 1985).

3. The  $\gamma$ -tail is due to Compton scattering by the nonthermal electrons and nonthermal bremsstrahlung. Since the optical depth of the nonthermal electrons is much less than unity due to Coulomb (see [5] below) and Compton cooling, the amplitude of the tail is much below that of the spectrum at lower energies. This results in a characteristic cutoff around 1 MeV. At large  $l_e$ , absorption in pair-producing photon-photon collisions further attenuates the  $\gamma$ -spectrum.

4. Bremsstrahlung is a source of soft photons always present in plasmas. In the absence of external (or synchrotron) soft

photons and at small compactnesses, the emitted spectra consist of thermal bremsstrahlung dominating at low energies, a pair annihilation feature at  $\epsilon \sim 1 + 3\Theta$ , and nonthermal bremsstrahlung dominating at high energies. At large compactnesses, the spectrum is mostly due to Comptonized thermal bremsstrahlung. The nonthermal bremsstrahlung emission is largely downscattered by the optically thick thermal pairs and absorbed in the process of photon-photon pair production.

5. Coulomb interactions are important in transferring energy from the nonthermal pairs to the thermal component of the plasma. The importance of this process increases with decreasing pair compactness,  $l_e$ , decreasing external soft photon input,  $l_s$ , and increasing power-law injection index,  $\Gamma$  (see Table 1). The relative importance of the Coulomb energy loss for an electron increases with decreasing  $\gamma$ . Coulomb interactions can transfer as much as one-half the power injected in primary nonthermal pairs to the thermal plasma. A consequence of the importance of Coulomb energy transfer is the small nonthermal Thomson depth ( $\tau_T^{\text{th}} \ll 1$ ) in photon-starved plasmas.

#### V. COMPARISON WITH OBSERVATIONS OF COMPACT OBJECTS

Some of the spectra from photon-starved plasmas resemble the spectra of classical  $\gamma$ -ray bursts. The continuum energy spectrum of those  $\gamma$ -ray bursts is roughly a broken power-law  $F_E \propto E^{-\alpha}$ , with an X-ray spectral index  $\alpha_x \sim 0$  and a  $\gamma$ -ray spectral index  $\alpha_\gamma$  varying from  $\sim 0.5$ –2 (Epstein 1986; Zdziarski 1987). The transition between the two regimes occurs between 100 keV and 1 MeV, suggesting some link between the shape of  $\gamma$ -ray burst spectra and the rest-mass energy of the electron. The *Solar Maximum Mission* data, which extend to  $\sim 5$ –10 MeV or more, show no clear high-energy cutoffs (Matz *et al.* 1985). The spectra shown in the dotted curve in Figure 1c, and the dotted and dashed curves in Figure 7, do show the broken power-law form.

On the other hand, the X-ray and  $\gamma$ -ray spectral indices for those spectra ( $\alpha_x \sim 0.4$ ,  $\alpha_\gamma \sim 1$ ) are perhaps slightly larger than those of typical bursts (Epstein 1986; Zdziarski 1987). Also, spectra from photon-starved plasmas require fine-tuning in order to reproduce the classical  $\gamma$ -ray burst spectra above a few hundred keV. Typical X-ray spectra from photon-starved plasmas do reproduce the  $\alpha_x \sim 0$  X-ray power-laws of  $\gamma$ -ray bursts, but those are then followed by spectral cutoffs by an order of magnitude at  $\sim 1$  MeV (see § III). This is not seen in the spectra of classical  $\gamma$ -ray bursts.

The so called soft  $\gamma$ -ray repeaters (SGRs) have spectra much softer than those of the classical  $\gamma$ -ray bursts. Those bursts include SGR 0526–66, the source of the 1979 March 5 event (Mazets *et al.* 1979; Cline *et al.* 1980), SGR 1900+14 (Mazets *et al.* 1982), and SGR 1806–20, the source of the 1979 January 7 event (Laros *et al.* 1986; Atteia *et al.* 1987; Laros *et al.* 1987; Kouveliotou *et al.* 1987). The bursts from these sources typically have color temperatures  $\sim 50$  keV, much less than that of other  $\gamma$ -ray bursts. Some of the spectra from photon-starved plasmas with large compactness may resemble those of soft  $\gamma$ -ray repeaters (see, e.g., the dotted curve in Fig. 1b).

Spectra from photon-starved plasmas are different from the typical X-ray spectra of active galactic nuclei, which have  $\alpha_x \sim 0.7$  (e.g., Mushotzky 1984). However, the few AGNs observed in soft  $\gamma$ -rays exhibit characteristic peaks at  $\sim 1$  MeV. It is possible that such peaks are typical of most of AGNs, since it does not violate the constraints imposed by the cosmic  $\gamma$ -ray

background (e.g., Bassani *et al.* 1985). In fact, a similar MeV peak followed by a steep power-law is seen in the isotropic cosmic background. Such peaks are characteristic of photon-starved plasmas and could come from AGN source components different than those responsible for the X-ray continua.

On the other hand, photon-starved plasmas can also explain spectra of AGNs that are harder than  $\alpha_x = 0.5$  (e.g., Mushotzky 1984). Such spectra cannot be explained by either the nonthermal synchrotron model or first-order Compton cooling models (see, e.g., Svensson and Zdziarski 1989).

This research was supported in part by NASA Grants NAGW-830 (Chicago), NAGW-1301 (Caltech), and NSF Grants AST 86-15325 and AST 84-51725 (Caltech). Two of us (D. Q. L. and A. A. Z.) are grateful for the warm hospitality of the Aspen Center for Physics, where part of this work was carried out. The authors acknowledge valuable comments and discussions with Alan Lightman, Roland Svensson, and Matthew Baring.

## APPENDIX

### RELATIVISTIC NONTHERMAL BREMSSTRAHLUNG

We use the bremsstrahlung cross section in the relativistic limit,  $\gamma \gg 1$ . It applies in the same form to  $e^\pm p$ ,  $e^\pm e^\pm$ , and  $e^+ e^-$  interactions. Here  $p$  denotes protons. In the laboratory frame,

$$\frac{d\sigma_B}{d\epsilon} = \frac{3\alpha_f}{2\pi} \sigma_T \frac{d\epsilon}{\epsilon} \frac{\gamma'}{\gamma} \left( \frac{\gamma'}{\gamma} + \frac{\gamma}{\gamma'} - \frac{2}{3} \right) \left( \ln \frac{2\gamma\gamma'}{\epsilon} - \frac{1}{2} \right). \quad (\text{A1})$$

Here  $\gamma'$  denotes the electron Lorentz factor after the photon emission,  $\gamma' = \gamma - \epsilon$ . In the case of  $e^\pm e^\pm$  and  $e^+ e^-$  interactions, this cross section gives the radiation from the fast electron only.

In treating the interactions of nonthermal pairs with themselves, we follow the approach of Zdziarski (1980). Using the fact that relativistic electrons emit radiation predominantly in the forward direction, we obtain

$$\dot{n}_B^{\text{nth, self}}(\epsilon) = \frac{1}{2} 2c \int_{\max(\gamma_{\text{th}}, \epsilon+1)}^{\gamma_{\text{max}}} N(\gamma_1) \frac{d\sigma_B}{d\epsilon_L} \frac{d\epsilon_L}{d\epsilon} d\gamma_1 \int_{\gamma_{\text{th}}}^{\gamma_{\text{max}}} N(\gamma_2) d\gamma_2 \int_0^1 \mu d\mu. \quad (\text{A2})$$

Here  $\epsilon_L$  and  $\epsilon$  are the laboratory frame and the plasma frame photon energies, respectively,  $\mu = (1 - \cos \vartheta)/2$ ,  $\vartheta$  is the collision angle, and  $d\sigma_B$  is a function of  $\gamma_L = 2\mu\gamma_1\gamma_2$ . Photons at energy  $\epsilon$  are radiated by electrons at  $\gamma_1$ . The factors 1/2 and 2 above account for the double counting of identical particles and the fact that both colliding particles radiate photons, respectively. The colinearity of the radiation emitted by relativistic pairs leads to the relation  $\epsilon_L/\gamma_L = \epsilon/\gamma$ . Except for the logarithmic term, the cross section (A1) is a function of factor  $\epsilon/\gamma$ , which is invariant. Only the factor  $\gamma$  in the argument of the logarithm is not invariant. Taking into account that  $\ln \gamma_L = \ln \gamma_1 + \ln \gamma_2 + \ln 2\mu$ , and neglecting the weak dependence on collision angle, we obtain the approximate relationship

$$d\sigma(\gamma_L) \simeq d\sigma(\gamma_1) + d\sigma(\gamma_2). \quad (\text{A3})$$

The photon production rate (A2) then simplifies to

$$\dot{n}_B^{\text{nth, self}}(\epsilon) = 2\tau_T^{\text{nth}} \frac{c}{\sigma_T R} \int_{\max(\gamma_{\text{th}}, \epsilon+1)}^{\gamma_{\text{max}}} N(\gamma) \frac{d\sigma_B}{d\epsilon} d\gamma. \quad (\text{A4})$$

In treating the interactions of nonthermal pairs with thermal pairs, we take the thermal particles to be at rest, and integrate the cross section (A1) over the distribution  $N(\gamma)$ . Using equation (A4), we can write the nonthermal bremsstrahlung emissivity from both self-interactions and interactions with thermal pairs in the compact form,

$$\dot{n}_B^{\text{nth}}(\epsilon) = \frac{c}{\sigma_T R} (\tau_T^{\text{th}} + 2\tau_T^{\text{nth}}) \int_{\max(\gamma_{\text{th}}, \epsilon+1)}^{\gamma_{\text{max}}} N(\gamma) \frac{d\sigma_B}{d\epsilon} d\gamma. \quad (\text{A5})$$

The fact that bremsstrahlung from relativistic electrons interacting with themselves is twice as large as that from relativistic electrons interacting with non-relativistic particles having the same density was noted earlier in the particular case of relativistic thermal plasmas (see, e.g., Haug 1975; Zdziarski 1980). Here we see that it also applies to relativistic nonthermal plasmas. The origin of this property is the logarithmic dependence on  $\gamma$  of the cross section (A1), which leads to the relationship (A3).

We obtain the bremsstrahlung cooling rate by integrating the cross section (A1) (e.g., Blumenthal and Gould 1970), and taking into account the result (A5),

$$\dot{\gamma}_B = -\frac{3\alpha_f}{2\pi} \frac{c}{R} (\tau_T^{\text{th}} + 2\tau_T^{\text{nth}}) \left( \ln 2\gamma - \frac{1}{3} \right). \quad (\text{A6})$$

The self-absorption frequency for nonthermal bremsstrahlung is given by a formula analogous to equation (20), but with  $\tau_T^{\text{th}}$  replaced by  $(\tau_T^{\text{th}} \tau_T^{\text{nth}})^{1/2}$  and  $\Theta$  replaced by the factor  $\sim \gamma$  ( $\sim 1$ ), appropriate to the lowest energy nonthermal electrons which dominate the nonthermal bremsstrahlung emission. Since thermal bremsstrahlung emission typically dominates over the nonthermal bremsstrahlung at  $\epsilon \ll 1$ , so does thermal bremsstrahlung self-absorption.

## REFERENCES

- Atteia, J.-L., *et al.* 1987, *Ap. J. (Letters)*, **320**, L105.  
 Bassani, L., Dean, A. J., Di Cocco, G., and Perotti, F. 1985, in *Active Galactic Nuclei*, ed. J. E. Dyson (Manchester: Manchester University Press), p. 252.  
 Blumenthal, G. R., and Gould, R. J. 1970, *Rev. Mod. Phys.*, **42**, 237.  
 Cline, T. L., *et al.* 1980, *Ap. J. (Letters)*, **237**, L1.  
 Coppi, P. S. 1990, *M.N.R.A.S.*, in press (C90).  
 Coppi, P. S., and Blandford, R. D. 1990, *M.N.R.A.S.*, in press (CB90).  
 de Kool, M., and Begelman, M. C. 1989, *Ap. J.*, **345**, 135.  
 Dermer, C. D., and Liang, E. P. 1989, *Ap. J.*, **339**, 512.  
 Done, C., and Fabian, A. C. 1989, *M.N.R.A.S.*, **240**, 81.  
 Epstein, R. I. 1986, in *Radiative Hydrodynamics in Stars and Compact Objects*, ed. K.-H. Winkler and D. Mihalas (Heidelberg: Springer), p. 305.  
 Fabian, A. C., Blandford, R. D., Guilbert, P. W., Phinney, E. S., and Cuellar, L. 1986, *M.N.R.A.S.*, **221**, 931.  
 Gould, R. J. 1975, *Ap. J.*, **196**, 689.  
 Guilbert, P. W., Fabian, A. C., and Rees, M. 1983, *M.N.R.A.S.*, **205**, 593.  
 Haug, E. 1975, *Zs. Naturforschung*, **30a**, 1546.  
 Kouveliotou, C., *et al.* 1987, *Ap. J. (Letters)*, **322**, L21.  
 Laros, J. G., *et al.* 1986, *Nature*, **322**, 152.  
 ———. 1987, *Ap. J. (Letters)*, **320**, L111.  
 Lightman, A. P., and Zdziarski, A. A. 1987, *Ap. J.*, **319**, 643 (LZ87).  
 Marshall, H., *et al.* 1980, *Ap. J.*, **235**, 4.  
 Matz, S. M., Forrest, D. J., Vestrand, W. T., Chupp, E. L., Share, G. H., and Rieger, E. 1985, *Ap. J. (Letters)*, **288**, L37.  
 Mazets, E. P., Golenetskii, S. V., Gur'yan, Yu. A., and Il'inskii, V. N. 1982, *Ap. Space Sci.*, **84**, 173.  
 Mazets, E. P., Golenetskii, S. V., Il'inskii, V. N., Aptekar', R. L., and Guryan, Yu. A. 1979, *Nature*, **282**, 587.  
 Mushotzky, R. F. 1984, *Adv. Space Res.*, Vol. 3, Nos. 10–12, p. 157.  
 Rybicki, G. R., and Lightman, A. P. 1979, *Radiative Processes in Astrophysics* (New York: McGraw-Hill).  
 Svensson, R. 1982, *Ap. J.*, **258**, 321.  
 ———. 1984, *M.N.R.A.S.*, **209**, 175.  
 ———. 1986, in *Radiation Hydrodynamics in Stars and Compact Objects*, ed. D. Mihalas and K.-H. Winkler (New York: Springer), p. 325.  
 ———. 1987, *M.N.R.A.S.*, **227**, 403.  
 Svensson, R., and Zdziarski, A. A. 1989, in *STScI-GSFC Workshop on Ultra-Hot Plasmas and Electron-Positron Pairs in Astrophysics*, ed. A. A. Zdziarski and D. Kazanas (Baltimore: STScI), p. 1.  
 Zdziarski, A. A. 1980, N. Copernicus Astronomical Center Preprint No. 115.  
 ———. 1984, *Ap. J.*, **283**, 842.  
 ———. 1985, *Ap. J.*, **289**, 514.  
 ———. 1987, in *13th Texas Symposium on Relativistic Astrophysics*, ed. M. P. Ulmer (Singapore: World Scientific), p. 553.  
 ———. 1988, *Ap. J.*, **335**, 786.  
 Zdziarski, A. A., and Lamb, D. Q. 1986, *Ap. J. (Letters)*, **309**, L79 (ZL86).  
 Zdziarski, A. A., and Lightman, A. P. 1985, *Ap. J. (Letters)*, **294**, L79.  
 ———. 1987, in *Variability in Galactic and Extragalactic X-Ray Sources*, ed. A. Treves (Milano: Associazione per l'avanzamento dell'astronomia), p. 121.

PAOLO S. COPPI: 130–33 Caltech, Pasadena, CA 91125  
 [INTERNET: coppi@tapir.caltech.edu]

DON Q. LAMB: Department of Astronomy and Astrophysics, The University of Chicago, 5640 South Ellis Avenue, Chicago, IL 60637  
 [INTERNET: lamb@oddjob.uchicago.edu]

ANDRZEJ A. ZDZIARSKI: Space Telescope Science Institute, 3700 San Martin Drive, Baltimore, MD 21218  
 [BITNET: zdziarski@stsci]